Photochemical and Acoustic Interactions of Biochar with CO_2 and H_2O: Applications in Power Generation and CO_2 Capture

Wei-Yin Chen
Dept. of Chemical Engineering, University of Mississippi, 134 Anderson Hall, University, MS 38677

Daniell L. Mattern
Dept. of Chemistry and Biochemistry, University of Mississippi, 322 Coulter Hall, University, MS 38677

Eneruvie Okinedo, James Corbett Senter, Alec A. Mattei, and Connor W. Redwine
Dept. of Chemical Engineering, University of Mississippi, 134 Anderson Hall, University, MS 38677

DOI 10.1002/aic.14347
Published online January 16, 2014 in Wiley Online Library (wileyonlinelibrary.com)

A critical literature review suggests that carbonaceous compounds react with (CO_2 + H_2O) mixture through thermal, photochemical, and sonochemical/sonophysical routes. A biochar was selected for studying these effects at 60°C and 1 atm for its potential benefits on power generation and CO_2 capture. All treatments remove sizable minerals (K, Na, and Si) detrimental in power generation, and introduce carbon (up to 16% of original carbon in biochar) into the biochar matrix. Most treatments show increased hydrogen (up to 24%). Treatments lead to notable increased heating value of biochar (up to 50%). Treated biochars show increase (up to 19 fold) in internal surface area. The ultrasound energy output is a fraction of the increased heating value. Thus, pretreatment is potentially attractive for increasing the energy efficiency in combustion and gasification. Moreover, better understandings of the salient reactions of these processes will be advantageous for the development of advanced adsorbents for CO_2 capture. © 2014 American Institute of Chemical Engineers *AIChE J*, 60: 1054–1065, 2014

Keywords: photochemical, sonochemical, CO_2 capture, water, biochar, gasification

Introduction

The current study synthesizes scientific observations and principles from disparate fields: chemical and photochemically induced CO_2 fixation on carbon, structural characteristics of biochar, solvent-induced swelling of carbonaceous materials, and acoustic physics and chemistry. Each of these will be described in the next four subsections, followed by a summary of the goals of the current work.

Known reactions of aromatic carbons with CO_2

Photocatalytic fixation of CO_2 on carbonaceous materials is a potentially attractive approach since it brings CO_2 to a higher energy state using renewable solar energy. Indeed, photo- and electrochemical conversion of CO_2 and H_2O have been identified as one of the top five research areas in catalysis that require urgent attention by the Department of Energys (DOE's) Basic Energy Sciences (Bell et al., 2007).[1] Photocatalytic conversions of CO_2, including those to fuels, have been recently reviewed by Kumar et al. and Izumi.[2,3] Among many types of reactions, a special category of CO_2 fixation is "reductive photocarboxylation" on aromatic compounds. This was first accomplished by Tazuke et al.[4,5] by Hg-lamp irradiation of a solution containing an aromatic hydrocarbon and CO_2, in the presence of a hydrogen donor, such as dimethylformamide, and an electron donor, such as N,N-dimethylaniline (DMA). In addition to undergoing carboxylation, the aromatic structures are reduced by the addition of hydrogen. A carbon-centered radical anion is the reaction intermediate induced by the lamp and the electron donor. Instead of using a liquid solvent, Chateauneuf et al.[6] used supercritical CO_2 in their reductive photocarboxylation experiments. The reaction equilibrium favors carboxylated product under high CO_2 pressure. Near complete conversion of anthracene was observed at 35°C and 2000 psi, with 2-propanol as a hydrogen atom donor, and DMA as the electron donor. About 57% of the product was dihydrocarboxylic acid. This carboxylation reaction can be stated as

$$\begin{aligned} &\mathrm{PAH} \xrightarrow{h\nu} \mathrm{PAH}^{*} + \mathrm{DMA} \rightarrow \mathrm{PAH}^{\bullet -} + \mathrm{CO_2} \\ &\rightarrow \mathrm{PAH}^{\bullet} - \mathrm{CO_2}^{-} + \mathrm{iPrOH} \rightarrow \mathrm{H-PAH-CO_2}^{-} \end{aligned} \tag{R1}$$

where PAH represents the polycyclic aromatic hydrocarbon. With respect to the chemistry, the key to this remarkably high conversion of anthracene rests on the role of the electron donor in forming the reaction intermediate, $PAH^{\bullet -}$, a

Correspondence concerning this article should be addressed to W. -Y. Chen, at cmchengs@olemiss.edu.

charged free radical, by electron transfer to the photochemically excited PAH.

In addition to the above photochemical reaction, carboxylation of aromatic carbon has been achieved thermally by the Kolbe-Schmitt reaction with an anion intermediate at around 100°C.[7–9]

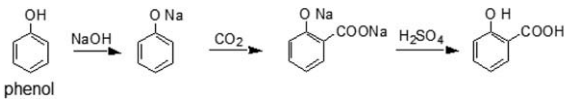

(R2)

or

$$RO^- + CO_2 \rightarrow ROCOO^- \quad \text{(R3)}$$

One of the objectives of this work is to investigate the extents of thermal (R2) and reductive photochemical (R1) carboxylation of carbonaceous materials containing PAH. These CO_2 fixation reactions could serve as the major step for CO_2 capture and CO_2 utilization. Reductive photochemical carboxylation brings PAHs to higher energy states and therefore, creates a cradle-to-cradle carbon cycle.

Biochar characteristics

The solid residue produced from the heating of lignocellulosics in inert gas is called biochar. Biochar is a byproduct of bio-oil production and has been gaining increasing attention because it is also a potent soil amendment and carbon sequestration medium.[10–12] As a soil amendment, it reduces soil acidity, adsorbs and immobilizes nutrients, and reduces greenhouse gas emissions (N_2O, up to 80%, and CH_4) from plants. More importantly, it is stable, with an average carbon half-life of 100 to 10^7 years, depending on the amounts of aliphatic and volatile components.[13] Due to its potentially large storage capacity in soil, it has been considered a major carbon storage method for mitigating climate change.

At the outset of this work, we decided to investigate the impacts of CO_2 on the chemical and physical structures of a carefully selected carbon substrate with the goal of identifying potentially attractive technologies in CO_2 capture and utilization. A biochar was selected for this study due to some of its structural characteristics. First, both biochar[14] and coal-derived chars[15] contain stacks of graphite clusters that contain graphene and graphene oxide (GO) layers whose edge carbons are reactive and could serve as binding sites for CO_2. Second, titanium dioxide in biochar is a known semiconductor; it could serve as the electron donor in photocatalytic reactions of aromatics and CO_2 such as those identified by Chateauneuf, et al.[6] Moreover, graphite is an electron conductor, which is likely to enhance the desired electron transfer. Third, using the phenol decomposition rate reported by Horn et al.,[16] the estimated decomposition of phenol at typical biochar preparation temperatures of 550°C, with a 10 min residence time, is about 4.2%. Thus, biochar is likely to retain a large quantity of phenols in the raw biomass that are susceptible to photochemical interactions with ammonia and amines.[17–19] Diamines, such as ethylenediamine (EDA), have been adopted in preparing adsorbents for capturing CO_2, with one amino group fixed on the substrate and the other free for capturing CO_2. The treatment of biochar with ammonia and amines (both photochemical and nonphotochemical) could lead to aminolysis on the surface that, in turn, would enhance the subsequent CO_2 capture. Plaza et al.[20] found that ammonia treatment (nonphotochemical) of biochar derived from almond shells at severe temperatures (400–900°C) generates stable functional groups that decompose to both NH_3 and HCN above 200°C. Fourth, Lee et al.[21] reported that the char derived from corn stover is rich in hydroxyl, carboxyl, and carbonyl groups, which are likely to react with NH_3 and amines. Fifth, the acidic ions of dissolved CO_2 in water can enhance the dissolution of metal ions in the biochar.

Finally, water and/or ethanol are known hydrogen donors that can serve as the desired source of hydrogen in the proposed photochemical fixation process.

Swelling of carbonaceous materials

It has been demonstrated that coal, biomass, and coal-derived chars can be swelled by solvents, including CO_2 and H_2O, after the breakage of cross-linkages in their macromolecular structure. Hydrogen bonds, especially those contributed by hydroxyl and carboxyl groups, have been considered as the major cross-links between aromatic clusters (e.g., Nishioka and Larsen;[22] Solomon et al.;[23] Larsen and Gurevich;[24] Larsen et al.[25]). Nucleophilic attacks of nitrogen-containing solvents are particularly effective in breaking these hydrogen bonds. Painter and coworkers,[26–28] conversely, suggest that the observed swelling is mainly caused by phase change, such as the intersection of a liquid–liquid phase separation and a glass-transition of the substrate. Their postulation is supported by the fact that the relaxation times of the hydrogen bonds in the liquid state, 10^{-11} to 10^{-5} s, is much shorter than that of a mechanical experiment such as swelling.

At temperatures as low as 298 K, CO_2 is known to induce significant irreversible swelling in coal volume by up to 4.18%, pore volume enlargement up to 50%, and depression in the glass-transition temperature from 120 to 82°C.[29–31] The extent of these effects increases with increasing temperature up to 200°C and pressure up to 30 atm (subcritical). Although, it is known that solvent-treated coals have higher reactivity in liquefaction[32–35] and swelled coal has a higher gasification rate,[36] the possible benefit of using solvent-treatment (such as CO_2) as a method of tuning carbon reactivity in combustion and gasification has not been explored. Recently, Gathitu et al.[37] found that supercritical CO_2 treatment of coals induces physical structure changes including swelling and increased internal surface area; moreover, it can also be adopted as a method for tuning the evolution of nitrogen from solid fuels and therefore, the NO formation in combustion.[38]

Sonochemistry and sonophysics

When a liquid is exposed to an ultrasonic (acoustic) field, the pressure waves of the sonic vibrations create a time/frequency dependent acoustic pressure, consisting of alternating compression, and rarefaction cycles.[39] If the applied pressure is equal to the negative pressure developed in the rarefaction cycle of the wave such that the distance between the molecules of the fluid exceeds the critical molecular distance to hold it together, the liquid breaks apart to form cavities made of vapor and gas-filled microbubbles. This acoustic cavitation consists of at least three distinct and successive stages: nucleation, bubble growth (expansion), and implosive collapse.[40,41] During the nucleation stage, cavitational nuclei are generated from microbubbles trapped in microcrevices of suspended particles within the liquid. During the collapse stage, the energy released is so extreme that the trapped gases undergo molecular fragmentation, which is the

underlying phenomenon in homogeneous sonochemistry. This collapse is accompanied by emissions of light, or sonoluminescence (SL).[42] Spectroscopic analyses of SL revealed that the temperature and pressure can reach up to 20,000 K and several thousand bar, respectively.

Sonication has been widely adopted to enhance mixing and reduce mass-transfer limitations in liquid/solid interactions, and in cleaning substances contaminated with fine particles inside their pores. Thus, it is likely that ultrasound is capable of removing fine mineral particles in the porous biochar and enhancing the desired reactions due to increased mass transfer in aqueous solution. Also, water splitting and the formation of oxygen, hydroxyl, and peroxyl radicals during the bubble-collapse stage of sonication render it attractive for oxidizing organic waste in water and oxidative desulfurization of fuels.[39]

Interestingly, Stankovich et al.[43] demonstrated that graphite oxide can be completely exfoliated by ultrasound (150 W) in phenyl isocyanate for 1 h, producing single-layer GO. Oxidation of graphite produces intercalated hydroxyl and epoxide groups and induces a disrupted sp^2–bonded carbon network, which is likely to happen during the preparation of biochar from biomass. Thus, sonication of biochar in a liquid solution could exfoliate the GO clusters and produce exposed layers. GO platelets are expected to be more reactive than graphitic oxide clusters due to the higher GO contact area.

Our interests in conducting ultrasound treatment include the possibilities of graphite oxide exfoliation in biochar, mineral removal, and water splitting. Exfoliation and mineral removal are expected to induce positive benefits on the heating value of biochar.

Objective and scope of the current work

The objective of this work is to enhance the fundamental understanding of CO_2 interactions with carbonaceous materials, especially CO_2 fixation on carbon, which is vital to the development of CO_2 capture and many utilization technologies. We report the impacts of photochemical and sonochemical treatments on biochar with (CO_2+H_2O). We were particularly interested in CO_2 fixation by photochemical and photocatalytic routes so that solar energy could be stored in the carbonaceous substrates. Ultrasound treatment was also included due to its potential of inducing mineral removal, exfoliation of graphite oxide, and GO clusters, and water splitting. It is also known that polar solvents, including H_2O and CO_2, are capable of swelling carbonaceous materials. Biochar has unique characteristics in structure and composition for the target reactions.

The synthesis of these discoveries led to a group of hypotheses concerning the changes in biochar after its treatment with CO_2 and H_2O under ultrasound and photochemical irradiation. The results reveal that pretreatment of biochar with CO_2 and H_2O can be beneficial to gasification efficiency. Moreover, one of the salient reactions suggests that GO may be a building block for the development of advanced adsorbents for capturing CO_2 from power generation. Systematic studies in the future are warranted.

In this work, we report both thermal and photochemical treatment of an aqueous suspension of biochar at 60°C and 1 atm in the presence and absence of saturated CO_2. The effects of magnetic stirring vs. the use of a sonicator are also examined. Treated and untreated biochars are characterized and compared. The scientific and technological implications of these results are discussed.

Experimental

Pyrolysis

Sorghum was ground and sieved to between 75 and 106 microns followed by drying under vacuum at 40°C overnight before pyrolysis. Biochar was produced in an alumina tube of 1.92 cm i.d. identical to that previously used for coal pretreatment.[38] The alumina tube was vertically placed in an electrically heated tube furnace with carrier gas He entering from the top. The carrier gas and volatile pyrolysis products exited from the bottom of the reactor tube, passed through a tee and then entered the exhaust hose horizontally. A stainless steel tube of 1.92 cm i.d. and 7.62 cm length was placed vertically at the other end of the stainless-steel tee for the collection of condensed bio-oil produced from pyrolysis by gravity. The bio-oil collector was capped at its bottom. The horizontal exhaust line was packed with glass wool for trapping bio-oil and avoiding contaminations of the transfer line in the downstream.

About 6.0 g of dried sorghum was wrapped in a 325 mesh stainless-steel screen and placed in the center portion (about 10.2 cm) of the alumina tube heated by an electrical tube-furnace with a 30.6 cm long heating element. This was done to minimize temperature differences of the sample in the axial direction.[44] Pyrolysis was conducted with a 5°C/min heating ramp to 550°C followed by a 10 min holding time. During pyrolysis, the sample was swept by He at 400 mL/min flow rate. The ultrahigh purity He was purified by copper turnings at 500°C in a furnace to remove any trace oxidants before entering the pyrolysis reactor.[45] The copper turnings were periodically regenerated by 30% CO balanced with He at 250°C for 20 min. A gas chromatograph/mass spectrometer was used to ensure that the oxidants in He were removed. After the pyrolysis, the biochar was then allowed to naturally cool to room temperature in flowing He before being removed from the reactor. About 2.0 g of biochar was produced from each pyrolysis experiment. The analyses of raw sorghum biochar are included in Tables 1 through 3.

Photochemical and thermal treatments

About 3.0 g of biochar (<100 μm) was mixed with 250 mL of deionized water in a 500-mL single-neck Pyrex flask with a stopcock septum port side arm. CO_2 (99.99%) was bubbled through some mixtures for 1 h, and those mixtures were then kept under equilibrium with CO_2 for 30 min. The sealed flask was then placed in a water bath. Treatments were conducted with either a 90 W aquasonic sonicator (VWR 75HT) of 38.5–40.5 kHz or a magnetic stirrer to enhance liquid/solid interactions. For photochemical reactions, light from a 250-W Xenon lamp (SLMLH450) was reflected into the flask by a mirror. The temperature of the water bath usually reached about 60°C during the irradiation. Tests were also conducted with the identical procedure at 60°C without irradiation, which is called the "thermal" treatment in the subsequent discussion. In preparing the thermally treated samples, no actions were taken to prevent the influences of fluorescent lamps used in the lab and natural sunlight that diffused through the windows. The sealed flask was allowed to cool and the treated char separated from the liquid solution using vacuum filtration. Samples were dried at 105°C overnight after filtration and then weighed.

For the study of the effects of sonication power output, selected sonication treatments were performed with much

Table 1. Changes in Weight, Chemical Elements, Heating Value, Surface Area and Metal Compositions of Biochar During *Magnetically-Stirred* Treatment with (CO2+H2O) at 65°C and 1 atm for 5 h*

Analysis/Samples	Rim Biochar (wt)	Thermally Treated wt %	Change during treatment (wt %)	Photochemically Treated (wt %)	Change during treatment (wt %)
Moisture[a]	6.95	7.2	–	5.66	–
Ash[a]	29.46	19.2	−43.0%	22.56	−33.0%
Fixed Carbon[a]	46.42	57.73	8.1%	55.53	4.1%
Volatiles[a]	17.28	15.87	−20.1%	16.25	−18.1%
Carbon[a,b]	55.35	64.85	1.9%	62.4	−1.9%
Hydrogen[a,b]	1.895	1.84	−16.0%	2.71	24.0%
Nitrogen[a,b]	0.595	0.62	−9.3%	0.81	18.0%
Oxygen[a,b] (by difference)	12.62	13.41	−0.1%	11.52	−0.3%
Sulfur[a,b]	0.08	0.08	−13.0%	< 0.05	>−45%
Organics[a]	70.54	80.8	−0.1%	77.44	−2.2%
Overall Weight Change (dried)	–	–	−13.0%	–	−12.0%
Atomic C/O ratio	5.85	6.45	10.3%	7.22	23.5%
Atomic H/O ratio	2.40	2.20	−8.6%	3.76	56.7%
BET Surface Area (m^2/g)	12.9	252.2	1855.0%	256.6	1889.1%
Heating Value (kcal/g)	4.83	5.63	16.6%	5.76	19.3%
K, % of total sample[a]	5.75	0.914	−91.0%	0.779	−92.0%
Na, wt ppm[a]	603	<445	>−58%	<411	>−61%
Si, % of total sample[a]	8.71	4.65	−70.0%	4.34	−57.0%

*The "thermally" and "photochemically" treatments differ by the use of Xe lamp irradiation during the treatment; no irradiation was used during the preparation of thermally treated sample.
[a]The Difference (%) in this row takes into account the overall mass change of the char during treatment. The reported difference represents the change in mass of the component and not the % difference of the numbers in the row.
[b]The ultimate analysis is reported based on dry sample.

shorter residence times, 3 and 12 min, and a larger quantity of dried biochar, 6 g. Other treatment conditions and procedures remained the same.

Characterizations

The early phase of this study revealed significant loss of minerals from the biochar after either photo or thermal treatment. Therefore, Si, Na, and K of biochar were quantified using inductive coupled plasma optical emission spectroscopy by Galbraith Laboratories. Ultimate and proximate analyses were conducted by Combustion Resources. Carbon, hydrogen, and nitrogen were analyzed by oxidizing the sample in pure O_2 by following ASTM5373. Total organic and inorganic sulfur was determined by high temperature combustion by following ASTM D4239. Oxygen was determined by difference. These data are presented in Tables 1 through 4.

The BET-N_2 isotherms were collected using a Quantachrome Instruments NOVA 1200 gas sorption analyzer running Firmware Version 3.70. Samples were degassed for 3 h at 300°C to eliminate debris, such as water, which clogs up pore space prior to the analysis. Equilibrium pressure tolerance was set at 0.1 mm Hg, equilibrium time tolerance 60 s, dwell time 240 s, and a thermal delay of 300 s was adopted.

Quantitative Fourier transform infrared (FTIR) transmission spectra of the samples were obtained using finely

Table 2. Changes in Weight, Chemical Elements, Heating Value, Surface Area and Metal Compositions of Biochar During Sonicated Treatment with (CO_2+H_2O) at 65°C and 1 atm for 5 h*

Analysis/Samples	Raw Biochar (wt %)	Thermally Treated (wt %)	Change during treatment (wt %)	Photochemically Treated wt %	Change during treatment (wt %)
Moisture[a]	6.95	2.16	–	2.36	–
Asha[a]	29.46	11.4	−70.2°%	11.8	−68.0%
Fixed Carbon[a]	46.42	70	16.1%	70.7	21.8%
Volatiles[a]	17.28	16.5	−26.4%	15.1	−30.1%
Carbon[a,b]	55.35	81.2	13.0%	80.1	15.8%
Hydrogen[a,b]	1.895	2.68	8.9%	2.66	12.3%
Nitrogen[a,b]	0.595	0.68	−12.0%	0.62	−17.0%
Oxygen[a,b] (by diffe rence)	12.62	3.98	−1.2%	4.76	−1.1%
Sulfur[a,b]	0.08	0.06	−42.2%	0.06	−40.0%
Organics[a]	70.54	88.6	−1.6%	88.2	0.0%
Overall Weight Change,%	–	–	−23.0%	–	−20.0%
Atomic C/O ratio	5.85	27.20	365.2%	22.44	283.7%
Atomic H/O ratio	2.40	10.77	348.4%	8.94	272.2%
BET Surface Area (m^2/g)	12.9	151.41	1073.7%	171.74	1231.3%
Heating Value (kcal/g)	4.83	7.26	50.3%	7.18	48.7%
K, % of total sample[a]	5.75	0.51	−97.4%	0.55	−97.0%
Na, w ppm[a]	603	456	−77.5%	<809	>58.5%
Si, % of total sample[a]	8.71	3.92	−86.6%	4.27	−76.2%

*The "thermally" and "photochemically" treatments differ by the use of Xe lamp irradiation during the treatment; no irradiation was used during the preparation of thermally treated sample
[a]The Difference (%) in this row takes into account the overall mass change of the char during treatment. The reported difference represents the change in mass of the component and not the % difference of the numbers in the row.
[b]The ultimate analysis is reported based on dry sample.

Table 3. Changes in Weight, Chemical Elements, Heating Value, Surface Area and Metal Compositions of Biochar During Sonicated Treatment with H_2O (no CO_2) at 65°C and 1 atm for 5 h*

Analysis/Samples	Raw Biochar (wt %)	Thermally Treated (wt %)	Change during treatment (wt %)	Photochemically Treated wt%	Change during treatment (wt %)
Moisture[a]	6.95	3.77	–	3.63	–
Ash[a]	29.46	12.4	−65.5%	13.1	−63.5%
Fixed Carbon[a]	46.42	61.4	8.6%	53.6	−5.3%
Volatiles[a]	17.28	22.4	6.3%	29.7	41.0%
Carbon[a,b]	55.35	75	11.1%	71.4	5.8%
Hydrogen[a,b]	1.895	2.54	9.9%	2.95	27.7%
Nitrogen[a,b]	0.595	0.67	−7.7%	0.76	4.7%
Oxygen[a,b] (by difference)	12.62	9.39	−0.6%	11.8	−0.4%
Sulfur[a,b]	0.08	0.05	−48.8%	0.05	−48.8%
Organics[a]	70.54	87.6	0.9%	86.9	0.5%
Overall Weight Change	–	–	−18.0%	–	−18.0%
Atomic C/O ratio	5.85	10.65	82.1%	8.07	38.0%
Atomic H/O ratio	2.40	4.33	80.1%	4.00	66.5%
BET Surface Area (m^2/g)	12.9	45.12	249.8%	76.94	496.4%
Heating Value (kcal/g)	4.83	6.76	40.0%	6.5	34.6%
K, % of total sample[a]	5.75	1.01	−93.9%	1.02	−93.9%
Na, w ppm[a]	603	< 851	>−54.3%	<684	>58.6%
Si, % of total sample[a]	8.71	3.7	>−85.3%	3.45	>−78.1%

*The "thermally" and "photochemically" treatments differ by the use of Xe lamp irradiation during the treatment; no irradiation was used during the preparation of thermally treated sample
[a]The Difference (%) in this row takes into account the overall mass change of the char during treatment. The reported difference represents the change in mass of the component and not the % difference of the numbers in the row.
[b]The ultimate analysis is reported based on dry sample.

ground samples pressed into KBr pellets. The pellets were prepared by a procedure established by Solomon and Carangelo.[46] Around 3 mg of char sample were mixed and ground with 1.8 g of KBr in a Wig-L-Bug shaker for 10 min. Around 0.15 g of the mixtures were pressed into pellets in an evacuated die under 20,000 lbs pressure. The pellets were stored in a desiccator for about a week. The pellet was analyzed in a Perkin-Elmer Spectrometer 1000. Heterogeneity of the small sample and complexities in pellet composition and handling procedure could cause discrepancies in such semiquantitative procedure. Thus, FTIR analysis was repeated till the spectra of at least six pellets from the same biochar sample had notable strong correlations. The actual number of spectra taken was 6 to 10. Then the averaged spectra of these six spectra were used in comparison of the raw and treated samples. Due to the complexity of the reactions involved in the treatments, it is not clear if there is a valid anchor in the IR spectrum that represents an unchanged functional group during the treatments. Thus, the three FTIR spectra of raw and treated samples were normalized over the entire region of wave number, 400–4300 cm^{-1}, for characterization.

Data presented in Tables 1 through 4 were averages of two analyses of the same sample to ensure that the difference was within 5%. Moreover, all data reported in Table 1 were averages of the results of two samples from two independent pyrolysis followed by treatment; reproducibility was also within 5% difference.

Results and Discussion

Magnetically stirred thermal and photochemical treatments

Changes in Sample Weight, Chemical Elements, Surface Area, and Heating Value. Table 1 presents the changes in weight, chemical elements, surface area, heating value, and metal compositions of biochar during magnetically stirred treatment with (CO_2+H_2O) at 65°C and 1 atm for 5 h. The interactions in a simple, magnetically stirred biochar/water/CO_2 system in our experiments are vigorous. Both photochemical and thermal treatments result in 12–13% loss in total weight, see Table 1. Proximate and ultimate analyses in Table 1 show significant losses in total mineral matters during the treatments. Specifically, thermally and photochemically treated biochars experience 43% and 32% losses in total ash content, respectively. It should be mentioned that the percentage changes of elements, volatiles, fixed carbon, total minerals (ash), total organics (the difference between the dried sample and total mineral), and the mineral species

Table 4. Changes in Weight, Chemical Elements, Heating Value, Surface Area and Metal Compositions of Biochar During Sonicated Treatment with H_2O and CO_2 at 65°C and 1 atm for 3 min

Analysis/Samples	Raw Biochar (wt)	Ultrasound Treated 3-min (wt %)	Difference (wt %)
Moisture[a]	6.95	4.07	–
Ash[a]	29.46	24.40	−25.8%
Carbon[a,b]	55.35	65.44	5.9%
Hydrogen[a,b]	1.895	1.84	−13.0%
Nitrogen[a,b]	0.595	0.61	−8.1%
Oxygen[a,b] (by difference)	12.62	7.62	−45.9%
Sulfur[a,b]	0.08	0.09	0.8%
Organics[a]	70.54	75.6	−4.0%
Overall Weight Change (dried)	–	–	−10.4%
Atomic C/O ratio	5.85	11.45	95.8%
Atomic H/O ratio	2.40	3.86	60.8%
BET Surface Area (m^2/g)	12.9	118.9	821.7%
Heating Value (kcal/g)	4.83	5.739	18.8%
K, % of total sample[a]	5.75	1.26	−83.74%
Na, wt ppm[a]	603	734	−9.67%
Si, % of total sample[a]	8.71	8.90	−24.17%

[a]The Difference (%) in this row takes into account the overall mass change of the char during treatment. The reported difference represents the change in mass of the component and not the % difference of the numbers in the row.
[b]The ultimate analysis is reported based on dry sample.

in Tables 1 through 4 are reported based on their content in the raw biochar.

It has been reported that minerals in biomass, coals, and their chars and fly ashes, such as K, Na, S, Cl, P, Mg, Ca, Fe, Al, and several trace metals, can be effectively removed by water at ambient conditions with or without externally introduced acid.[47–52] The chemistry and mass-transfer limitations in leaching minerals from fly ashes was reviewed by Iyer.[53] It is expected that the dissolved CO_2 enhances the acidity of water and therefore, the dissolution of mineral ions in aqueous solutions. Thus, the loss in total weight during treatments is mainly due to the dissolution of minerals in the aqueous solution. Interestingly, it was recently discovered that water leaching of biochars results in about 2% organic carbons extracted in the leachate.[54] If these organic acids, such as acetate, formate, and oxalate, stay in a batch reactor, the organic acids can help remove the minerals in the biochar.[55] A reactor with a continuous-flow water does not enjoy such benefits.

Inductively coupled plasma optical emission spectrometry analysis of metals in the biochars indicates that 70% of Si, 91% of K, and at least 58% of Na are removed from biochar during thermal treatment. About 57% of Si, 92% of K, and at least 61% of Na are removed from biochar during photochemical treatment. We have noted the losses of these minerals earlier in the treatment of lignite by supercritical CO_2.[37,38] The technological significance of mineral removal in the process will be discussed in a later section.

While the treatments remove roughly 33–43 wt % minerals in biochar, calculations based on ultimate analysis, see Table 1, show 0.1 to 2.2% weight losses of the organics into the aqueous phase during thermal and photochemical treatments, respectively. This level of loss of organics was also observed in our previous SC CO_2 treatment of coals.[37,38] Table 1 indicates that organic oxygen is one of the elements contributing to the weight loss during the photochemical treatments.

Ultimate analysis shown in Table 1 also reveals that photochemical treatment leads to notable, 57% higher, atomic H/O ratios, in contrast to thermal treatment that shows a 9% decrease in atomic H/O ratio. Photochemical and thermal treatments result in 24 and 10% increases in atomic C/O ratio of biochar, respectively. The notable increase in hydrogen content during the photochemical treatment suggests that the sample is hydrogenated during photochemical treatment, and Reaction R1 discussed in Section I.D may indeed have taken place during the photochemical treatment. In this process, TiO_2 in biochar, not an amine as used by Chateauneuf et al.[6] in Reaction R1, may have served as an electron donor, and water may have served as a hydrogen donor. The small changes in carbon and oxygen content and atomic C/O ratios during both treatments do not provide substantial indication of whether carbon is fixed on the biochar, or oxygen is removed from the biochar.

These simultaneous removals of minerals, and increases in H/O ratios, during the photochemical treatment suggest that photo irradiation of a biochar/water/CO_2 system is likely to enhance the heating values of biochars. Indeed, heating value of biochar shown in Table 1 increased by 17 and 20% during thermal and photochemical treatment, respectively. Calculations show that the increase in heating value is not solely from loss of mineral matter. The 24% weight increase of hydrogen during the photochemical treatment, as shown in Table 1, suggests that hydrogenation contributes to the increase in the heating value as well.

The 16% loss in hydrogen during the thermal treatment suggests biochar undergoes different reaction mechanisms during the photochemical and thermal treatments. The decrease in hydrogen also explains the slightly lower heating value of biochar after thermal treatment. The increase in biochar's heating value during photochemical treatment implies that renewable solar energy is stored in biochar during treatment, which is a highly desirable outcome.

BET data shown in Table 1 suggest that the two treatments induce about 19-fold increases in internal surface area, suggesting swelling during the treatments. Such increases in surface area, in turn, imply that the treated biochars are likely to have much higher reactivity than the parent biochar during fluid/solid reactions. As discussed in the Introduction, the observed increase in internal surface area is likely caused by breakage of hydrogen bonds and phase change. Previous works on CO_2-induced swelling of coals were also summarized in the Introduction.

The observations from the characterizations discussed above are likely to have significant technological implications to steel and power industries, which will be discussed in a later section.

Implications from Fourier-transform Infrared and Other Analysis. The FTIR spectra of raw and thermal or photochemically treated (magnetically stirred with CO_2) biochars are shown in Figure 1. As discussed in the earlier sections, the complexity and unknown nature of the reacting system do not allow us to choose a particular peak as the anchor in the normalization procedure. Therefore, we used a scaling factor to minimize the overall difference between reference and treatment spectra, which made them superimpose if treatment caused no change, and looked for peaks that were anomalously high or low, indicating functional groups that changed.

Using this normalization, the wavelength region between 2800 and 1800 cm^{-1}, where the signal should be blank for all three samples, showed definite differences between treated (decreased) and control. This gives us a qualitative measure of the uncertainties of this analysis; as a practical matter, those differences give us a boundary for significance. That is, changes similar in size to those in the blank region will not be very compelling. We also minimized spectral differences omitting the blank region. The results were similar, except for changes occurring around 1100 cm^{-1}.

The most convincing changes are decreases upon treatment at 700 and 750 cm^{-1}, regions for aromatic C***-H patterns. These changes would be consistent with substituting other groups for edge, aromatic C-H. However, the changing aromatic substitutions would be expected to give increasing peaks in the same region (700–900 cm^{-1}), which is not observed. Decreases upon treatment at 700 and 750 cm^{-1} could also be due to the loss of Si-C bands. Nevertheless, it is not likely that SiO_2 in the biomass is converted to SiC at 550°C during pyrolysis followed by subsequent SiC loss during treatment.

Around 1600 cm^{-1} there is a small increase for thermally treated and a slightly larger increase for photochemically treated biochars. The changes here are at the boundary of significance, but they would be consistent with the formation of carboxylate groups during the treatments. The signal differences are small and follow-up studies will be needed.

The IR analysis does not support obvious increases in CH stretching intensities, so it does not provide confirmation of hydrogenation or aldehyde formation.

The photochemical treatment of biochar under an atmosphere of CO_2 leads to a small decrease in oxygen, as

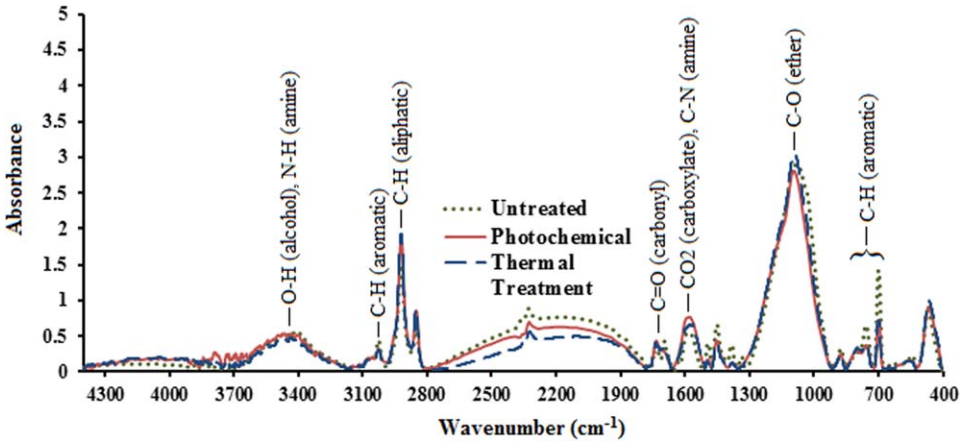

Figure 1. FTIR absorbance spectra of raw biochar (green), thermally treated biochar (blue), and photochemically treated biochar (red).

Treatments were performed with a magnetic stirrer in the flask. A scaling factor is used to minimize the overall difference between reference and treatment spectra. Small increases in wavelength 1600 cm^{-1} could be consistent with the hypothesis that carboxylation during the treatments gives carboxylate groups. The most notable changes are decreases upon treatments at 700 and 750 cm^{-1}, regions for aromatic C-H patterns. These changes would be consistent with substituting other groups for edge, aromatic C-H. [Color figure can be viewed in the online issue, which is available at wileyonlinelibrary.com.]

reflected in increased H/O and C/O ratios and increased heating values. One possibility is that a photoreduction (formally a hydrogenation), such as the one modeled below for an aryl lactone present in the complex structure of the biochar, could be occurring. The photoreduction could be assisted by TiO_2 or silicates present in the biochar.

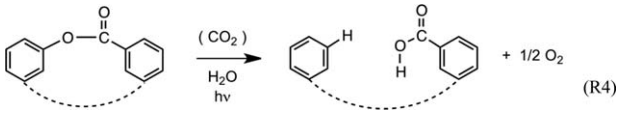

(R4)

The FTIR spectra suggest that carboxylation, such as the ones modeled in R1, R2, R3, R4, and R5 (below) for a diaryl ether present in the complex structure of the biochar, could be occurring.

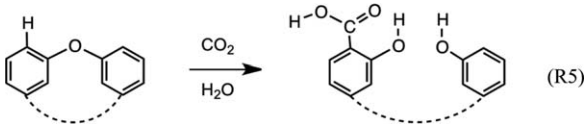

(R5)

However, heating values rise for thermally treated biochar, suggesting reduction, and O/H ratios fall; neither result is explained by carboxylation. Thus, several simultaneous processes may be occurring, the most interesting of which are carboxylations (for sequestration of CO_2) and reductions (for converting biochar/CO_2 into higher-energy forms).

Sonicated thermal and photochemical treatments with CO_2

Changes in Sample Weight, Chemical Elements, Surface Area, and Heating Value. Table 2 presents the changes in weight, chemical elements, surface area, heating value, and metal compositions of biochar during sonicated treatment with (CO_2+H_2O) at 65°C and 1 atm for 5 h. Its shows a 23% and 20% decreases in overall weight for the thermal and photochemical treatments, respectively, when ultrasound is used during the experiments. The ultrasound-induced weight losses come mainly from the mineral matters portion of the biochar. Table 2 shows 70 and 68% weight losses of ash for the thermal and photochemical treatments, respectively. These losses of minerals are significantly higher than that of the magnetically stirred tests shown in Table 1. Metal analysis reveals about 97, 78, and 86% losses of K, Na, and Si into the leachate during the thermal treatments, respectively. The photochemical treatment removes 97, 59, and 76% losses of K, Na, and Si into the leachate, respectively. These loses are slightly higher than

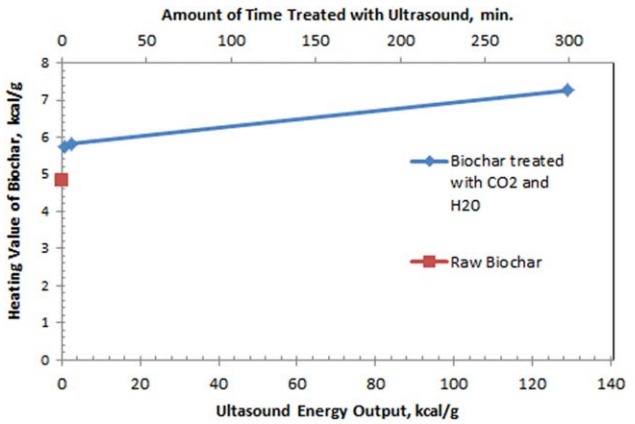

Figure 2. Benefits of ultrasound power to biochar's heating value.

Biochar treated with (CO_2+H_2O) and 90-W ultrasound shows notable increases in heating value. The 3-min treatment results in a 19% increase in heating value. The majority of the ultrasonic energy is consumed by environment surrounding the reactor; cavity formation consumes only a small fraction of the energy in the current apparatus. In practice, ultrasonic energy can be most efficiently used by directly inserting a high powered ultrasonic horn in the solution in the treatment reactor. Thus, the data from tests with short treatment times indeed suggests the potential energy and economic benefits of installing a biochar treatment reactor prior to gasification or combustion. [Color figure can be viewed in the online issue, which is available at wileyonlinelibrary.com.]

those for the magnetically stirred experiments, and suggest that there might be higher ultrasound-induced losses of mineral elements that are not included in the current study. It is known that K and Na form organometallic bonds in biochar that can be removed by acidic ions. Ultrasound enhances the mass transfer and therefore, the leaching.

Biochar also loses 1.6% of weight of the organic portion (the combustibles) in the thermal treatment. The loss in organics during the combined thermal and photochemical treatments is negligible. These levels of small losses are comparable to those for the magnetically stirred experiments.

Ultrasound induces negligible amounts of oxygen during the two types of treatments. Nevertheless, the gains in both hydrogen and carbon elements in both thermal and photochemical treatments are high and notable. Specifically, ultrasound induces a 9 and 12% gain of hydrogen in thermal and photochemical treatments, respectively. It also induces a 13 and 16% gain of carbon in thermal and photochemical treatments, respectively. These element changes result in 3.5- and 2.7-fold increases in atomic H/O ratio during thermal and photochemical treatments, respectively. They also correspond to 3.7- and 2.8-fold increases in atomic C/O ratio in thermal and photochemical treatments, respectively. The increased carbon content suggests carbon capture by biochar during the treatments.

Comparing the elemental analysis data of photochemically treated sample in Table 1 and those of thermally treated sample in Table 2 (with ultrasound), it can be concluded that the photochemical treatment leads to higher (24.0%) hydrogen gain than ultrasonic treatment (8.9%). Moreover, ultrasonic treatment leads to a higher (13.0% gain) carbon change than photochemical treatment (1.9% loss). Combined photochemical and ultrasonic treatment, shown in Table 2, leads to a 12.3% and 15.8% of hydrogen and carbon gain, respectively.

The losses of minerals and gain in hydrogen and carbon suggest an increase in heating value of biochar during the treatments. Indeed, the heating value of biochar increases by 50 and 49% during the thermal and photochemical treatments, respectively. These increases are significantly higher than those observed in the experiments with a magnetic stirrer, which show 17 and 20% increases during the thermal and photochemical treatments, respectively.

Ultrasound induces 11- and 12-fold increases in BET surface area during the thermal and photochemical treatments, respectively. Although, it is a significant increase, it is lower than the 19-fold increase observed in magnetically stirred experiments, suggesting the weak correlation between the changes in chemical elements due to reactions and BET surface area. As discussed in the next section, it has been demonstrated that ultrasound effectively exfoliates the graphite oxide in the production GO. Thus, this observed "moderate" increase in surface area could be due to the exfoliation of graphite oxide clusters in biochar that results in the filling of mesopores by exfoliated GO platelets. It should be mentioned that this increase in internal surface area remains much higher than previously observed CO_2-induced swelling in dried coal[29–31] at temperatures up to 200°C and pressure up to 30 atm (subcritical), which suggests the synergism caused by the presence of water in biochar swelling.

Roles of Ultrasound. The discussions above suggest that ultrasound induces chemical and physical impacts on the system. Biochar has microcrevices that facilitate the formation of acoustic cavitation. The collapse of microbubbles induces high temperature and pressure that could significantly reduce mass-transfer limitations of fluid into the micropores. It also known that water splits into highly reactive H• and OH• radicals during the collapsing stage of microbubbles, which, in turn, induces formation of oxygen, peroxyl, and hydroxyl radicals. The strong oxidation power of these free radicals has been adopted in treating waste water that contains organic contaminants (e.g., Ince et al.,[41]). For the system under current investigation, however, it seems to be the hydrogen radicals that react vigorously with the oxygen functional groups on the internal surfaces of biochar. Moreover, the observed 13 and 16% increase in carbon content shown in Table 2 for the thermal and photochemical treatments, respectively, seem to suggest the possible occurrences of reactions such as R1 through R5 discussed above.

As discussed in the Introduction, the clusters of graphite and graphite oxide in biochar could be exfoliated and form graphene and GO platelets during sonication.[43] The observed enhancement in reaction levels reported in Table 2 may also be contributed by the exfoliation of graphite oxide clusters in biochar, which facilitates the attack of edge carbons of graphene. The ultrasound-treated samples show lower increases in internal surface area than those mixed by magnetic stirring, see Tables 1, 2. The observed decrease in BET surface area could be a result of filling the mesopores with exfoliated graphene and GO platelets during the ultrasound treatment.

Finally, ultrasound-induced mass transfer is likely to play a significant role in the system. It is expected acidic ions in the solution of CO_2 and H_2O can react with the metallic ions of the organometallic matrix and remove them from the biochar. Thus, the synergism of using ultrasound is also expected, as evidenced from the observed mineral removals during the treatment.

In summary, ultrasound seems to have induced a group of synergistic processes that happen simultaneously during the treatment: exfoliation of GO and graphite clusters, chemisorption of CO_2 on biochar, mineral leaching, and hydrogenation. These benefits were expected at the outset of this study, as discussed in the Introduction. More importantly, all these processes cause increase in heating value of the biochar.

Roles of Light. There is no major disparity in heating value and surface area between the thermally treated and photochemically treated treatments when mixed with a sonicator. However, their elemental compositions and IR spectra discussed earlier are notably different, suggesting the possible involvement of different reaction pathways in the two treatments.

Hydrogen content shown in Tables 1, 2 suggest light alone induces 24% hydrogenation. Thus, the reductive photochemical CO_2 fixation mechanism proposed by Chateauneuf et al.[6] (Reaction R1 in Section ***I.A) could cause hydrogenation and a moderate (19%) increase in heating value. However, photo-irradiation alone does not seem to induce exfoliation of GO and graphite clusters, chemisorption of CO_2 on biochar, or additional mineral leaching. Only combined ultrasound and light induce the carbon fixation.

Effects of Sonication Energy Output. The 5-h treatment time used for most of the experiments in the current study was chosen to test our hypothesis that ultrasound would induce notable physical and chemical changes to biochar.

During the 5-h, 3-g experiment, the 90-W sonicator consumed 129 kcal per gram of biochar, that is, about 17 times of the heating vale of the raw biochar. To examine the feasibility of adopting the pretreatment in a practical gasification process, especially one that uses CO_2, rather H_2O, as the solid-fuel carrier, two experiments were performed with 6 g of biochar and with much shorter 3 and 12 min sonication times. The heating values of these treated biochars are compared with that of the raw biochar and that from the 5-h experiment in Figure 2.

As illustrated in Figure 2, short ultrasound-treatment time, for example, 3 min, resulted in a 19% increase in heating value. The energy consumed by the sonicator during the 3-min treatment was 0.65 kcal/g, which is less than the increase in heating value of the biochar, 0.91 kcal/g, during the 3-min treatment (from 4.83 to 5.74 kcal/g). Although the energy gain (the difference of these two energy quantities) seems to be limited, it is expected that a majority of the ultrasound energy is dissipated in its surroundings through several modes in the current apparatus, in which cavity formation consumes only a small fraction of the energy. In practice, ultrasonic energy can be most efficiently used by directly inserting a high powered ultrasonic horn in the solution in the treatment reactor. Thus, the data from tests with short treatment times indeed suggests the potential benefits in energy efficiency and economics of installing a biochar treatment reactor prior to gasification or combustion, which is discussed in a later section.

In Figures 1 through 4, a direct comparison between heating values of the samples before and after treatment was used in the calculation of gain/loss of heating value based on unit mass of the raw and treated biochar, respectively. This comparison is chosen to illustrate the benefit of treatment of the biochar before it enters a power generation process. It is not the percentage change in heating value of one unit weight of the raw char. The change in raw biochar's heating value would be a gross effect of a group of processes in the treatment, including loss of minerals and changes in carbon, hydrogen and oxygen contents, due to extraction, fixation and reactions.

Table 4 shows changes in weight, chemical elements, heating value, surface area, and metal compositions of biochar during sonicated treatment for 3 min with H_2O and CO_2 at 65°C and 1 atm. The results show that the sample loses about 10% of its overall weight. The biochar loses 26 and 4% of its overall ash and organic content, respectively. The treatment leads to a 6% increase in carbon content and 13 and 46% decrease in H and O content, respectively. When the 19% increase in heating value is compared to the decrease of ash content from 29 to 24%, it is clear that the increase in heating value is not solely contributed by the loss of mineral matter. The 6% carbon incorporation is the second contributor. The notable decreases in H and O are likely to have affected the heating values, too. More than an 8-fold increase in internal surface area was observed. K, Na, and Si showed 84, 10, and 24% decreases during the treatment.

Sonicated thermal and photochemical treatments without CO_2

Table 3 presents the changes in weight, chemical elements, surface area, heating value, and metal compositions of biochar during sonicated treatment with H_2O (no CO_2) at 65°C and 1 atm for 5 h. Thermal and photochemical experiments were conducted without CO_2 for investigating the role of CO_2. As shown in Table 3, with a few exceptions, most changes in treatments without CO_2 fall between those shown in Tables 1 and 2. This observation suggests the concerted roles of biochar, CO_2, H_2O, and ultrasound in chemical reactions.

Table 3 shows 18% weight loss for both the thermal and photochemical treatments. The significant ash losses for both treatments in Table 3 further support the sonicator's role in enhancing interactions between inorganics and the aqueous phase. Losses of measured mineral species K, Na, and Si, are about the same among the data shown in Tables 1 through 3, suggesting their weak dependency on CO_2, photo-irradiation and ultrasound.

The 11 and 6% carbon gain for the thermal and photochemical treatments, respectively, also fall between their counterparts in sonicated and the magnetically stirred systems with added CO_2. These observed gains in carbon reveal the possible range of analytical errors; nevertheless, it is also possibly due to the fast absorption of atmospheric CO_2 into the aqueous solution during sample handling. The basic nature of biochar can enhance the dissolution of CO_2 in aqueous solution. The gains of hydrogen, 10 and 28% for the thermal and photochemical treatments, respectively, in the system without CO_2 are highest among the three systems. This observation suggests the vigorous role of water in sonicated (biochar+water) systems. The remarkably high hydrogen gain, 28%, in the photochemical treatment suggests the possible ultrasound-induced photo-hydrogenation reactions without CO_2, that is, reactions other than R1 and R4. One possible reaction is the light-induced interaction between H• radicals and biochar.

The water leaching of organic acids from biomass and biochar were recently reported by Wu et al.[54] and Liaw and Wu[55] in their effort to recover inorganic nutrients from biomass and biochar. Although data in Table 4 show carbon fixation on the biochar, our pH measurements suggest that organic acids may be extracted by water during the treatments. The pH of the deionized water with biochar is 10.60, while the leachates from thermal and photo-chemical treatments of biochars have pH values 8.94 and 8.29, respectively.

The thermal and photochemical treatments without CO_2 lead to 40 and 35% increases in the heating value, respectively. These values are between the two other systems, which are the results of combined changes in carbon and hydrogen, and mineral removal.

BET surface area shows the smallest increase in this treatment without CO_2, although thermal and photochemical treatments still generate 2.5- and 5.0-fold increases in internal surface areas, respectively. Compared to the larger increases in BET surface area during sonicated treatment with CO_2, the concerted actions of CO_2 and water in biochar swelling are obvious. As in the other treatments, the surface area increase is greater for photochemical treatments than for thermal treatments, supporting again light's important role in the swelling of the char. Table 3 also shows that when CO_2 is absent, light plays an even larger role in the swelling of char. Specifically, the photochemical increase in surface area is twice that of the thermal case, a much larger disparity than that found in either CO_2 treatment.

Technological implications

Impacts on Combustion and Gasification. The observed changes in biochar properties after thermal and

photochemical treatments have technological implications. Combustion is the major current technology for disposing biochar. If implemented, the treatment technology is likely to significantly enhance its thermal efficiency. The 19–50% gain in heating value of biochar observed in the sonicated thermal treatment is likely to benefit the steel industry, in which biochar is used for energy production. Residual heat is usually available in a power plant that can provide the 60°C used in the treatment; indeed, the US Department of Energy's Innovation for Existing Plants program is looking various novel means for recovering the residual (or waste) heat from the cooling tower of the power plants.[56] Future power plants are expected to have CO_2-capture facilities for its subsequent storage and utilization.

It has been reported that coal-derived chars[15] and petroleum coke (e.g., Yen et al.[57]) both have graphene structures cross-linked by ethers and esters. Thus these carbonaceous materials are likely to possess similar benefits of increase in heating values, but at different levels, during the sonochemical treatment discussed here.

The observed aqueous leaching of K, Na, and Si is likely to be beneficial to power plants. Si significantly inhibits coal gasification rates (e. g., Yuan et al.[58]), and the high-volatility K and Na cause fouling and slagging in gasifiers and combustors.[36] Thus, the removal of minerals during treatment will lead to fewer operational problems during a power generation process. Nevertheless, Na and K are known catalysts in coal gasification, and significant losses of these alkali metals may induce unexpected adverse effects on the gasification rate. Recently, Ramsurn[59] found that addition of $Ca(OH)_2$ in the hydrothermal carbonization followed by addition of K_2CO_3 in hydrothermal gasification significantly enhance the rate of biochar gasification efficiency. One interesting aspect of the proposed pretreatment technology is that we will be able to control the amounts of recycled leachates, water and CO_2, and therefore the recycled metals, fed into the gasifier.

It has been demonstrated that significant amounts of soil nutrients, K and Na, appear in the leachate during water leaching of biochar.[54,55] (H_2O+CO_2) leaching of biochar under ultrasound and photochemical irradiation render it possible to recycle even higher amounts of mineral nutrients for soil originally present in the biomass. The fate of organic acids in the leachate remains a subject for future studies.

The treated biochar shows remarkable increases in internal surface areas, which, in turn, implies higher reaction rate or energy throughput in a combustor and gasifier.[36]

Impacts on Carbon Capture. CO_2 interactions with carbonaceous materials, either functionalized or unfunctionalized, is a versatile and potentially fruitful subject for the development of advanced carbon-based adsorbents for CO_2 capture. Only a few examples are discussed in this subsection.

As discussed in the Introduction, CO_2 fixation on the edge carbons of PAH through thermal and photochemical reactions may be a potentially viable new route for capturing CO_2 by carbonaceous materials. The Kolbe-Schmitt reaction, R2, mentioned above can be considered as a starting point. Regeneration can be achieved by decarboxylation under a moderate heat and/or vacuum. The heat of decarboxylation of *para*-hydroxybenzoic acid is 29 kJ/mol,[60] which is within a reasonable range for regenerating amine-based liquid absorbents. Carbon-based adsorbents have much lower heat capacities that allow low energy consumption in regeneration. Carbon-based sorbents usually have a higher resistance to SO_2 in flue gas among sorbents, which make them attractive for CO_2 capture.

The CO_2-aromatic carbon interactions discussed above can be related to the emerging and versatile research field of nanosized GO; GO has emerged as a major building block of many chemicals. Particularly worth noting is that amines have been successfully grafted on the two major oxygen functional groups on GO: carboxylic acids and epoxides.[61] It is anticipated that the GO functionalized by polyamines such as tetraethylenepentamine, EDA, polyethyleneimines, and hyperbranched amines with proper activation can be very attractive CO_2-capture adsorbents. For instance, Zhao et al.[62] demonstrated 5.4% CO_2 capture capacity of graphite oxide impregnated with EDA at 30°C and $P_{CO2} = 0.15$ atm. The capture efficiency is expected to be higher if GO (not graphite oxide) is adopted and if it is properly activated.

Separately, it has been demonstrated that O_2 can be photochemically fixed on PAH in the formation of phenol;[63] phenol is an important functional group for the synthesis of GO framework (GOF).[64] High porosity GOF materials with strong intercalated chemical linkages between the graphene layers as pillars have been synthesized and tested for CH_4 and H_2 storage and CO_2 capture.[64,65] Molecular simulations have demonstrated that polar groups such as COOH and NH_2 bonded to edge carbons of graphene significantly enhance CO_2 capture capacity.[66] Graphene without these functional groups showed a high, 35 wt %, CO_2 capture capacity at 195 K and 1 atm CO_2.[67] Although these experiments were not conducted at practically viable conditions for capturing CO_2 from power plants, they may be the initial attempt of a new route that warrants attention in the near future. Both semiconductors (e.g., TiO_2) and guest impurities (e.g., C and N atoms) can be impregnated onto substrate (carbon and metal) surfaces in one step at low temperature to enhance photo-electron activity by reducing the band gap of photo-reaction and therefore enhance photocatalytic reactions.[68] While photo-carboxylation can be adopted as a CO_2 capture technology, further treatment of photocarboxylated graphene by impregnating diamines (one amino group at each end of the compound) can induce higher CO_2 capture capacity.[69] These studies reveal that functionalized nanographenes and GOFs will be playing a pivotal role in this study. Photochemical and chemical treatment at moderate temperatures can be adopted either in the CO_2 capture process or in the production of adsorbents.

Finally, the treatments discussed in the current work were conducted with pure CO_2 at 1 atm. The observed benefits are likely to be even higher under high pressures, such as supercritical (CO_2+H_2O) conditions. Future power plants are expected to have compressed CO_2 at liquid state for transportation and storage. Moreover, sonochemistry can be adopted in treatment and sorbent regeneration in the CO_2 capture process discussed above, an area which has yet to be systematically studied.

Conclusions

Biochar treated with ultrasound and light, in CO_2/H_2O at 60°C and 1 atm, underwent the following remarkable changes: the significant removal of minerals (Si, K, and Na) detrimental to power generation, a 16-fold increase in internal surface area, a 9% addition of hydrogen and 13%

addition of carbon, and up to a 50% increase in heating value. The surface area changes suggest the exfoliation of GO clusters, producing GO platelets; the observed high CO_2 uptake by biochar may be partly due to exfoliated graphitic clusters. The 13% carbon fixation during the sonication treatment may be considered a new carbon capture or utilization process. FTIR suggests that carboxylation may accompany the chemical changes. The increase in heating value appears to be a combined result of mineral removal, carbon fixation, and, in some cases, hydrogenation. The gains in heating value and internal surface area of biochar after treatments indicate a potential increase in energy throughput in combustion and gasification.

These observations suggest that the governing reactions involved could greatly benefit the development of three major technologies: solid fuel pretreatment prior to gasification that uses CO_2 as the solid-fuel carrier; CO_2 capture by biochar or by functionalized nanoGO; and the recovery of inorganic nutrients for soil amendments. The application of the understanding of the sonochemical and photochemical reactions of (carbon+CO_2+H_2O) systems can be extended to pretreatment for combustion in addition to gasification and potential extension to other biomass studies. Since coal-derived chars and petroleum cokes have structures similar to biochar, the observed benefits for biochar are likely to be applicable to power generation based on these feedstocks too.

Acknowledgments

This work was supported by the University of Mississippi's Office of Research and Sponsored Programs through its regrant form the US Small Business Administration, SBAHQ-10-1-0309, Sally McDonnell Barksdale Honors College, Shao-Pong Chen's Honorary Research Fund, and Department of Chemical Engineering. We also appreciate the technical supports of William R. Meredith.

Literature Cited

1. Bell AT, Gates BC, Ray D. *Basic Research Needs*: *Catalysis for Energy*. Washington, DC: Office of Basic Energy Science, US Department of Energy, 2007.
2. Kumar B, Llorente M, Froehlich J, Dang T, Sathrum A. Photochemical and photoelectrochemical reduction of CO_2. *Annu Rev Phys Chem*. 2012;63:541–569.
3. Izumi Y. Recent advances in the photocatalytic conversion of carbon dioxide to fuels with water and/or hydrogen using solar energy and beyond. *Coord Chem Rev*. 2013;257:171–186.
4. Tazuke S, Ozawa H. Photofixation of carbon dioxide: formation of 9,10-dihydrophenanthrene-9,carboxylic acid from phenanthrene-amine-carbon dioxide systems. *J Chem Soc, Chem Commun*. 1975;7: 237–238.
5. Tazuke S, Kazama S, Kitamura N. Reductive photocarboxylation of aromatic hydrocarbons. *J Org Chem*. 1986;51:4548–4553.
6. Chateauneuf JE, Zhang J, Foote J, Brink J, Perkovic MW. Photochemical fixation of supercritical carbon dioxide: the production of a carboxylic acid from a polyaromatic hydrocarbon. *Adv Environ Res*. 2002;6:487–493.
7. Kolbe H. Ueber Synthese der Salicylsäure. *Ann Chem Pharm*. 1860; 113:125–127.
8. Schmitt R. Beitrag zur Kenntniss der Kolbe'schen Salicylsäure Synthese. *J Praktische Chem*. 1885;31:397–411.
9. Lindsey AS, Jeskey H. The Kolbe-Schmitt reaction. *Chemistry*. 1957;57:583–620.
10. Lehmann J, Joseph S. Biochar for environmental management, Science and Technology. United Kingdom: Earthscan, 2009.
11. Sohi S, Lopez-Capel E, Krull E, Roland B. Biochar, climate change and soil: a review to guide future research. CSIRO Land and Water Science Report. Commonwealth Scientific and Industrial Research Organisation, Australia, 2009.
12. Levine J.G. *US-Focused biochar report: assesment of biochar's benefits for the United States*. Center for Energy and Environmental Security, Boulder, Colorado, 2010.
13. Zimmerman A. Abiotic and microbial oxidation of laboratory-produced black carbon (biochar). *Environ Sci Technol*. 2010;44: 1295–1301.
14. Hammes K, Schmidt MWI. Changes of biochar in soil. In: Lehmann J, Joseph S, editor. *Biochar For Environmental Management, Science and Technology*. United Kingdom: EarthScan, 2009.
15. Franklin R. Crystallite growth in graphitizing and nongraphitizing carbons. *Math Phys Sci*. 1951;1097:196–218.
16. Horn C, Roy K, Frank P, Just T. Shock-tube study on the high-temperature pyrolysis of phenol. *27th Int Symp Combustion*. 1998: 321–328.
17. Ishiuchi S, Saeki M, Sakai M, Fujii M. Infrared dip spectra of photochemical reaction products in a phenol/ammonia cluster: examination of intracluster hydrogen transfer. *Chem Phys Lett*. 2000;322:27–32.
18. Ishiuchi S, Sakai M, Daigoku K, Hasimoto K, Fujii M. Hydrogen transfer dynamics in a photoexciteed phenol/ammonia (1:3) cluster studied by picosecond time-resolved UV-IR-UV ion dip spectroscopy. *J Chem Phys*. 2007;127:234304-1-234304-8.
19. Carrera A, Nielsen D, Carcabal P, Dedonder C, Broquier M, Jouvet C. Biradicalic excited states of zwitterionic phenol-ammonia clusterss. *J Chem Phys*. 2009;130:024302-1-24302-8.
20. Plaza MG, Pevida C, Martin CF, Fermoso J, Pis JJ, Rubiera F. Developing almond shell-derived carbons as CO2 adsorbents. *Sep Purif Technol*. 2010;71:102–106.
21. Lee JW, Kidder M, Evans BR, Paik S, Buchanan AC III, Garten CT, Brown RC. Characterizations of biochars produced from cornstovers for soil ammendment. *Environ Sci Technol*. 2010;44:7970–7974.
22. Nishioka M, Larsen JW. Association of aromatic structures in coals. *Energy Fuels*. 1990;4:100–106.
23. Solomon PR, Serio MA, Despande GV, Kroo E. Cross-linking reactions during coal conversion. *Energy Fuels*. 1990;4:42–54.
24. Larsen JW, Gurevich I. A method for counting the hydrogen-bond cross-links in coal. *Energy Fuels*. 1996;10:1269–1272.
25. Larsen JW, Flowers RA, Hall PJ, Carlson G. Structural rearrangement of strained coals. *Energy Fuels*. 1997;11:998–1002.
26. Painter P. Some comments concerning the solvent swelling of coal and coal extracts. *Energy Fuels*. 1992;6:863–864.
27. Painter P, Shenoy S. A new model for the swelling of coal. *Energy Fuels*. 1995;9:364–371.
28. Painter P. Some comments on the paper of Larsen et al. and the nature of cross-linking in coal. *Energy Fuels*. 1996;10:1273–1275.
29. Reucroft PJ, Patel H. Gas-induced swelling in coal. *Fuel*. 1986;65: 816–820.
30. Reucroft PJ, Sethuraman AR. Effect of pressure on carbon dioxide induced coal swelling. *Energy Fuels*. 1987;1:72–75.
31. Mirzaeian M, Hall PJ. Thermodynamical studies of adsorption / desorption of CO2 on the Wydak coal at different pressures. *Prepr Pap – Am Chem Soc, Div Fuel Chem*. 2007;52:20–25.
32. Bockrath BC. Chemistry of hydrogen donor solvents. In: Gorbaty ML, Larsen JW, Wender I, editors. *Coal Science*, Vol. 2, New York: Wiley-Interscience, 1983.
33. Pullen JR. Solvent extraction of coal. In: Gorbaty ML, Larsen JW, Wender I, editors. *Coal Science*, Vol. 2, New York: Wiley-Interscience, 1983.
34. Chen WY, Kazimi FM. Coal liquefaction with supercritical ammonia and amines. In: Penninger JML, McHugh MA, Radosz M, Krukonis VJ, editors. *Supercritical Fluid Technology*, Netherlands: Elsevier Science Publishers BV, 1985:281–307.
35. Chen WY, Kazimi FM. Coal liquefaction in primary aliphatic amine systems. *Ind Eng Chem Res*. 1990;29:1109–1119.
36. Wall TF, Liu GS, Wu HW, Roberts DG, Benfell KE, Gupta S, Lucas JA, Harris DJ. The effects of pressure on coal reactions during pulverized coal combustion and gasification. *Prog Energy Combustion Sci*. 2002;28:405–433.
37. Gathitu BB, Chen WY, McClure MC, Effects of coal interaction with supercritical CO2: physical structure. *Ind Eng Chem Res*. 2009; 48:5024–5034.
38. Gathitu BB, Chen WY. Effects of pretreatment of coal by CO2 on nitric oxide emission and unburned carbon in various combustion environments. *Ind Eng Chem Res*. 2009;48:10364–10374.
39. Mason TJ, editor. *Chemistry with ultrasound. Critical reports on applied chemistry, 28, society for chemical industry*, London: Elsevier, 1990.

40. Guo Z, Zheng Z, Zheng S, Hu W, Feng R. Effect of various sono-oxidation parameters on the removal of aqueous 2,4-dinitrophenol. *Ultrason Sonochem*. 2004;12:461–465.
41. Ince NH, Tezcanli G, Belen RK, Apikyan IG. Ultrasound as a catalyzer of aqueous reaction systems: the state of the art and environmental applications. *Appl Catal B*. 2001;29:167–176.
42. Suslick K, Flannigan J. Inside a collapsing bubble: sonoluminesence and the conditions during cavitation. *Annu Rev Phys Chem*. 2008;59: 659–683.
43. Stankovich S, Dikin DA, Dommett GHB, Kohlhaas KM, Zimney EJ, Stach EA, Piner RD, Nguyen ST, Ruoff RS. Graphene-based composite materials. *Nature*. 2006;442:282–286.
44. Chen WY. Rate measurement with a laboratory-scale tubular reactor. *Chem Eng Educ*. 1999;33:238–243.
45. Chen WY, Wan S, Shi G. Stable surface oxides on chars and impact of reactor materials at high temperatures. *Energy Fuels*. 2007;21: 778–792.
46. Solomon PR, Carangelo RM. FTIR analysis of coal: techniques and determination of hydroxyl concentrations. *Fuel*. 1982;61:663–669.
47. Jenkins BM, Bakker RR, Wei JB. On the properties of washed straw. *Biomass Bioenergy*. 1996;10:177–200.
48. Turn SQ, Kinoshita CM, Ishimura DM. Removal of inorganic constituents of biomass feedstocks by mechanical dewatering and leaching. *Biomass Bioenergy*. 1997;12:241–252.
49. Steenari BM, Schelander S, Lindqvist O. Chemical and leaching characteristics of ash from combustion of coal, peat and wood in a 12 MW CFB – a comparative study. *Fuel*. 1999;78:249–258.
50. Li Z, Moore TA, Weaver SD. Leaching of inorganics in the cretaceous Greymouth coal beds. *Int J Coal Geol*. 2001;47:235–353.
51. Arvelakis S, Vourliotis P, Kakaras E, Koukios, E.G. Effect of leaching on the ash behavior of wheat straw and olive residue during fluidized bed combustion. *Biomass Bioenergy*. 2001;20:459–470.
52. Ahmad I, Khan MA, Shakirullah M, Ishaq, M. Effect of leaching time on the removal of lithophile elements of operational concern from coal samples. *J Chem Soc Pak*. 2004;26:107–110.
53. Iyer R. The surface chemistry of leaching coal fly ash. *J Hazard Mater*. 2002;B93:321–329.
54. Wu H, Yip K, Kong Z, Li CZ, Liu D, Yu Y, Gao X. Removal and recycling of inherent inorganic nutrient species in mallee biomass and derived biochars by water leaching. *Ind Eng Chem Res*. 2011; 50:12143–12151.
55. Liaw S, Wu H. Leaching characteristics of organic and inorganic matter from biomass by water: differences between batch and semi-continuous operations. *Ind Eng Chem Res*. 2013;52:4280–4289.
56. US Department of Energy. Innovative Water Reuse and Recovery, Available at: http://www.netl.doe.gov/technologies/coalpower/ewr/water/innovative.html.
57. Yen TF, Erdman JG, Pollack SS. Investigation of the structure of petroleum asphaltenes by x-ray diffraction. *Anal Chem*. 1961;33: 1587–1594.
58. Yuan S, Chen XL, Li J, Wang FC. CO2 gasification kinetics of biomass char derived from high-temperature rapid pyrolysis. *Energy Fuels*. 2011;25:2314–2321.
59. Ramsurn H, Sandeep K, Gupta RB. Enhancement of biochar gasification in alkali hydrothermal medium by passivation of inorganic components using Ca(OH)2. *Energy Fuels*. 2011;25:2389–2398.
60. Bonneau-Gubelmann I, Michel M, Besson B, Ratton S, Desmurs J. Carboxylation of hydroxy aromatic compounds. *Ind Chem Libr*. 1996;8:116–128.
61. Dreyer DR, Park S, Bielawski CW, Ruoff RS. The chemistry of graphene oxide. *Chem Soc Rev*. 2010;39:328–340.
62. Zhao Y, Ding H, Zhong Q. Preparation and characterization of aminated graphite oxide for CO2 capture. *Appl Surf Sci*. 2012;258: 4301–4307.
63. Kawahata T, Otomo J, Oshima IY, Koda S. Photo-oxygenation of benzene in supercritical CO2. *J Supercrit Fluids*. 1998;13:197–204.
64. Burress JW, Gadipelli S, Ford J, Simmons JM, Zhou W, Yildirim T. Graphene oxide framework materials: theoretical predictions and experimental results. *Angew Chem Int Ed*. 2010;49:8902–8904.
65. Stankovich S, Dikin DA, Dommett GHB, Kohlhaas KM, Zimney EJ, Stach EA, Piner RD, Nguyen ST, Ruoff RS. Graphene-based composite materials. *Nature*. 2006;442:282–286.
66. Wood BC, Bhide SY, Dutta D, Kandagal VS, Pathak AD, Punnathanam SN, Ayappa KG, Narasimhan S. Methane and carbon dioxide adsorption on edge-functionalized graphene: a comparative DFT study. *J Chem Phys*. 2012;137:054702.
67. Ghosh A, Subrahmanyam KS, Krishna KS, Datta S, Govindaraj A, Pati SK, Rao CNR. Uptake of H2 and CO2 by graphene. *J Phys Chem C*. 2008;112:15704–15707.
68. Raveendran P, Fu J, Wallen SL. Completely "green" synthesis and stabilization of metal nanoparticles. *J Am Chem Soc*. 2003;125: 13940–13941.
69. Tanthana J, Chuang SSC. *in situ* infrared study of the role of the PEG in stablizing silica-supported amines for CO2 capture. *ChemSusChem*. 2010;3:957–964.

Manuscript received July 8, 2013, and revision received Oct. 8, 2013.